Prototyping of thin shell wind tunnel models to facilitate experimental wind load analysis on curved canopy structures.

Jimmy COLLIERS[abc], Marijke MOLLAERT[d], Joris DEGROOTE[e], Lars DE LAET[f]

[a]PhD – fellowship, Research Foundation Flanders (FWO), Egmontstraat 5, 1000 Brussel, Belgium

[b]PhD, Vrije Universiteit Brussel (VUB), Department of Architectural Engineering, Pleinlaan 2, 1050 Brussel, Belgium

[c]PhD, Universiteit Gent (UGENT), Department of Flow, Heat & Combustion Mechanics, Sint-Pietersnieuwstraat 41, 9000 Gent, Belgium

[d]Prof. dr. ir., Vrije Universiteit Brussel (VUB), Department of Architectural Engineering, Pleinlaan 2, 1050 Brussel, Belgium

[e]Prof. dr. ir., Universiteit Gent (UGENT), Department of Flow, Heat & Combustion Mechanics, Sint-Pietersnieuwstraat 41, 9000 Gent, Belgium

[f]Prof. dr. ir.-arch., Vrije Universiteit Brussel (VUB), Department of Architectural Engineering, Pleinlaan 2, 1050 Brussel, Belgium

Corresponding author: jimmy.colliers@vub.be

Abstract

The topologies of membrane and shell structures are not covered by existing wind load Standards and wind tunnel testing should be used to obtain representative wind loads for these structures. However, accurate scale-models of these organically shaped and often open thin structures are complex, time-consuming and expensive to build. To stimulate experimental research on wind load distributions over these structures, this paper illustrates a prototyping methodology for double curved thin shell wind tunnel models with integrated pressure sensors. The production process is illustrated for a hyperbolic paraboloid roof structure. The obtained wind load distributions are validated with literature for a flat roof and canopy that is made according to the same methodology and for two hyperbolic paraboloid roofs. Results indicate that, compared to conventional wind tunnel models, these thin shell wind tunnel models yield more realistic wind pressure distributions over very thin canopy structures. Finally, Cp-distributions are shown for the hyperbolic paraboloid canopy with the high corner under attack. The production of glass-fibre reinforced composites in a CNC-milled mould is convenient and accurate and facilitates the production of wind tunnel models to be used for wind load measurements on organically shaped thin canopy structures.

Keywords: Double curved models, Pressure measurements, Prototyping, Tensile surface structures, thin shell models, Wind tunnel models

1. Introduction

The use of tensile surface structures has increased significantly during last decades. Compared to the conventional heavy weight building roof topologies, these lightweight membrane structures are more sensitive to external loading, as a result of the low self-weight-to-load-ratio. In addition, the structural engineer has to deal with uncertainties in wind load estimations for these organically shaped flexible structures, because Standards for the calculation and dimensioning of membrane structures subjected to wind loading do not exist. Currently, wind loading on tensioned surface structures is often based on rough approximations referring to conventional building topologies of the existing Standards, which do not account for the special nature of the textile covers.

1.1. Wind loads on double curved structures

The need for extensive wind analysis on these double curved structures has been stressed in several international publications [1][2], stating the lack of the current standards (ASCE/SEI 7-05 [3] and EN 1991-1-4:2005 [4]) in governing the wind-resisting strength for these structures and the need for an industry-wide set of standards. From this point of view a lot of research on the wind loading of membrane structures is still required. Moreover, appropriate wind pressure data is essential to provide confidence in the analysis and design process, and to ensure the development of building codes that will facilitate the safe and efficient design of membrane structures as well as for double curved shell structures.

In general, conventional codes on wind design give upper bound values for the majority of structures, but the level of uncertainty increases as the building configuration deviates from the codified norms. For these cases, the Standards point out Wind tunnel testing as complementary or alternative approach to obtain load and response information for complex structures that are not covered in the code itself. Currently also Computation Fluid Dynamics is being used for these studies, but requires proper experimental validation by scaled wind tunnel testing or real scale measurements [5].

For double curved structures experimental wind tunnel testing is limited to a few cases. In particular wind load distributions are investigated for some conical membrane roofs [6][7] and some hyperbolic paraboloid (hypar) membrane roofs [8]-[13]. Some studies investigate only the overall lift coefficients of a roof obtained from a single load cell as for example in [14]. Furthermore, a wide variety of wind tunnel tests have been performed for

some specific case studies, mainly large-scale structures [15]-[17], stadium roofs [18] and cable-roofs [19]. Next to these experimental studies, numerical investigations using CFD have been performed for double curved membrane roof structures. Some pressure distributions are shown for hypars [14][20] and umbrella-like cones [21][22]. However, most of the numerical studies focus rather on the dynamics of these structures including fluid structure interaction coupling frameworks [22]-[26] and vibrations analyses [27]. The majority of the above-mentioned numerical studies, except for [14] and [23], include some experimental validation for the wind load determinations. Despite all these very specific experimental and numerical studies, only a few Cp-distributions are available over the basic shapes of membrane structures.

In order to tackle this shortfall extensive additional studies and tests on wind analysis for hypars, cones, arch forms and wave types are required. In addition, previous wind tunnel studies are considering these structures mainly in an enclosed configuration as a building roof, but they are mainly used as open free-standing canopies with a thickness of between 1 tot 2 mm. Therefore, this research establishes a hybrid rapid prototyping methodology for the production of double curved thin shell wind tunnel models in order to obtain more realistic wind pressures and Cp-values over these very thin canopy structures. The established methodology allows the production of wind tunnel models of only 5 mm thick with 62 integrated pressure taps that allow simultaneous pressure measurements on the upper and lower face of the shell, where models in other studies with similar amount of pressure taps are typically around 2 cm thick [43]. The reduction in thickness is (only) 4 times, but for scale models at typical wind tunnel scales that consider the influence of surrounding buildings this reduction in thickness becomes more important and especially for open canopies where the flow has to pass underneath the roof. On a scale of 1/500 for example, a 20 mm thick model would refer to a roof thickness of 1m, while a 5mm thick model refers to only 25 cm. For a canopy that is typically placed at a height of 3 m, the 20mm thick model would block 1/3th of the opening under the canopy, while a 5cm thick model would block only $1/12^{th}$ of the opening under the canopy. The methodology is developed in such a way that it can be adopted in a straight forward manner for all possible double curved thin shell shapes to facilitate wind tunnel testing towards wind load distributions over the basic double curved structures.

1.2. Wind tunnel prototype manufacturing

In wind engineering, wind tunnel testing is commonly considered as alternative to the conventional building Standards, especially for wind design of complex structures that fall outside the existing expertise. Wind tunnel

testing on scaled models is used to predict and/or improve the structural reliability of unusual aerodynamic and/or flexible structures under wind loading. In order to obtain and extrapolate representative and correct information from scaled wind tunnel experiments to full-scale structures, the experiments must meet certain criteria of the similarity theory taking into account model similitude and consistency of length scales. However, due to the limitations of scaling and modelling one may deviate from the strict similarity theory to simplify the wind tunnel models to partial or approximate substitutes, considering the concession-accuracy relation to the full-scale reality [28]. For more elaborated information on wind tunnel testing is referred to [5][28]-[30].

Due to the highly complex, time-consuming and expensive prototyping of wind tunnel models, relevant wind tunnel testing on Cp-distributions is very limited and only performed for few basic membrane shapes and some large-scale case studies like stadia. Traditional wind tunnel models are made out of metal with conventional machining operations (5-axis CNC-milling and grinding), take months to produce and cost thousands of dollars [31][32]. Recent studies show that rapid prototyping is emerging for making wind tunnel models [33]. Additive manufacturing techniques such as 3D-printing and selective laser sintering, can produce good results in agreement to the traditional metal models, with significant lower costs and production time [34]-[36]. However, in wind tunnel testing these models are mainly used in combination with a force balance yielding only the overall drag and lift coefficients. For overall pressure distributions, the model should be equipped with pressure taps, small holes on the surface connected with airtight passageways to the pressure transducers. The addition of these pressure taps is a particularly expensive and time-consuming job done by skilled workers.

1.3. Problem statement

Almost all models for wind tunnel testing in the field of aerodynamics and pressure distributions are enclosed rigid models that monitor Pressure Coefficients (Cp) at one face only. These models are generally produced to study wind load distributions in the built environment, where the building envelope usually encloses the pressure scanner. The pressure scanner connects to the pressure taps on the envelope and measures the pressure distribution over the outer face (Figure 1a). For membrane topologies these models could be made with various materials including wood, acrylic plastic and plaster [6]-[19]. One commonality is that all models are entirely handcrafted. In general, pressure distributions are shown in literature, but the model construction and materialisation are barely discussed. Nonetheless this is also particularly important to facilitate further

experimental research towards pressure distributions over double curved shapes. Therefore, this paper discusses a methodology to make thin shell double curved canopies with integrated pressure taps.

For the intended wind tunnel experiments that monitor Cp simultaneously on both faces of a thin shell model it is impossible to implement the pressure scanner in the model itself due to the slenderness of the model. The pressure scanner should be placed outside the model and preferably outside the wind tunnel to not disturb the airflow around the model. Air channels should be implemented in the model connecting the pressure taps with the pressure scanner (Figure 1b). These models are much more complex to build. In [6] such models are made from two layers of acrylic plastic with copper tubes in between. An important drawback of this technique is the need of pre-shaping and assembling all elements, what is quite labour intensive, results in rather thick canopy models and puts limits on the range of shapes.

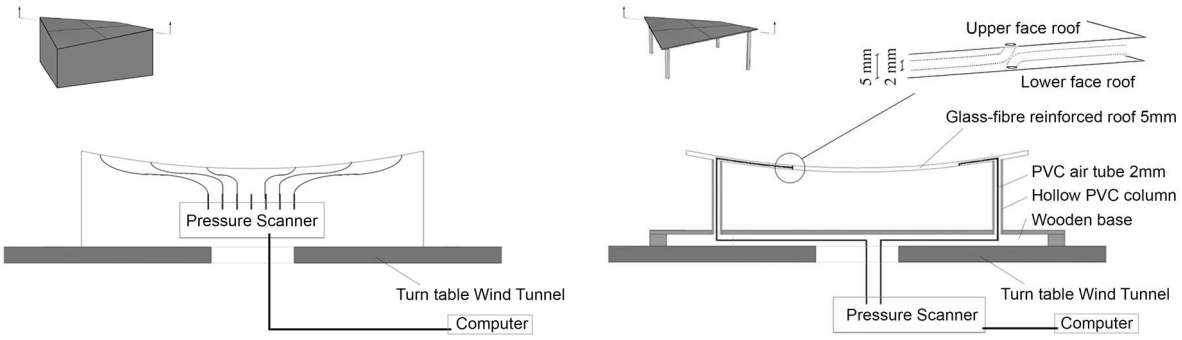

a. Typical wind tunnel model with pressure scanner inside. Cp-values are only measured on the outside of the envelope.

b. Intended wind tunnel model with pressure scanner underneath. Cp-values are measured on both sides of the shell.

Figure 1: Wind tunnel testing set-up.

Furthermore, since the pressure distribution depends on the geometrical factors of the structure, rigid models are used for structures that deform very little under wind loading, while aeroelastic models should be used to investigate flexible structures. However, properly scaled aeroelastic models representing a membrane structure are barely used because they are very complex to design and build. The flexibility of these structures depends on the interaction between membrane stiffness, applied pre-stress and supporting system, which are almost impossible to scale accordingly. For example, the technical textiles that are used for these structures are coated orthogonally woven fabrics with a thickness of approximately 1mm and often pretensioned with only 1 kN/m width of the fabric. This corresponds to a thickness of 0.1 mm and a pretension of 0.1 kN/m width of the fabric at a scale of 1/10 and knowing that for aerodynamic studies of the built environment scales of 1/100 up to 1/500

are not unconventional, it can be considered as impossible to scale these textiles and or mimic their properties accordingly. To overcome this problem, the flexible behaviour and corresponding deformations can be approximated by iterative wind tunnel testing on rigid models. Therefore, a rigid model with the initial geometry is made. The model is placed in the wind tunnel and Cp-values are recorded. The deflected geometry of the structure is calculated with the recorded Cp-values using computational structural dynamics. A new model is made with the deflected geometry and put in the wind tunnel. This process is repeated until Cp-values converge. This iterative approach stresses the need for convenient and accurate prototyping of complex double curved thin shell wind tunnel models. It is obvious that this latter approach is more suitable for numerical testing, however, proper experimental validation or real scale measures are required for these novel studies.

2. Prototyping of wind tunnel models

The production process is discussed for a rigid double curved thin shell hypar model with a square ground plan of 400 by 400 mm and a height of 50 mm (Figure 2). The scale of the model 1/25, representing a hypar roof of 10 m by 10 m and 1.25m high. Next to this slightly curved hypar, a higly curved hypar is made, with the same square ground plan and a height of 120 mm instead of 50 mm. The hypar shape is chosen because it is the most fundamental double curved shape of membrane structures. However, the proposed methodology can be applied in a straightforward way to other double curved shapes as well as to flat or planar shapes.

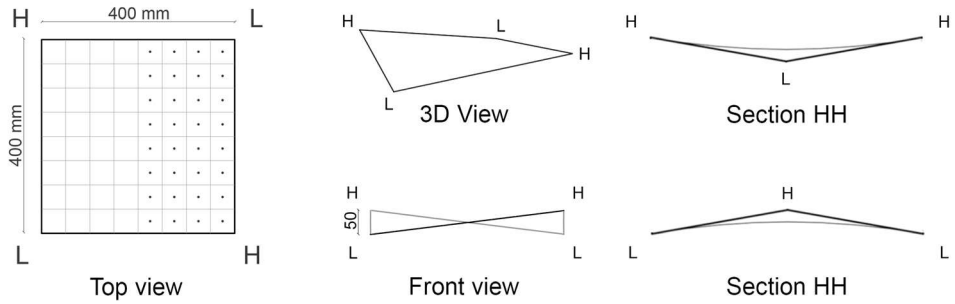

Figure 2: dimensions of hypar.

2.1. Model specifications

Most important model specifications for the double curved thin shell roof models are:

- simultaneous pressure measurement on both faces of the roof,
- possibility to test the models as part of a building roof and as a canopy,
- keep the thickness of the shell as low as possible.

The double curved thin shell models should allow simultaneous pressure measurement on both faces of the model (Figure 1b), where commonly used wind tunnel models only have pressure taps on the outside face of an enclosed volume (Figure 1a). The measuring points on both faces of the shell should be perfectly aligned for accurate summation of the Cp-values on both sides for canopy roofs.

The models will be tested as a roof structure that is part of the building envelope and as an open canopy structure, respectively with and without enclosing walls, and this for different angles of attack. Roof structures that are part of the building envelope will respond differently to the dynamic wind pressure compared to open canopy structures. Consequently, the former cannot be used as surrogate for the latter, even though open canopies are harder to model.

The thickness of the testing models has to be reduced as much as possible to approximate the mainly single-layer membrane structures, as the thickness of the roof boundaries will affect the airflow and thus the turbulence over the membrane. The thickness of a membrane usually ranges between 1 to 2 mm, which is impossible to scale in a wind tunnel model. By contrast, the minimal dimensions of the wind tunnel models are defined by the diameter of a typical model pressure tap (1-2 mm) [5] and the embedded Polyvinylchloride (PVC) tubes that connect to the measuring sensors of the pressure scanner. These tubes have an outer diameter of 2 mm. Moreover, the PVC tubes should connect perpendicular to the roof surface, referring to the nature of wind pressure acting perpendicular to surfaces. Therefore, an additional 2 mm is required to bend the tubes without necking. Taking into account the additional material for surface finishing and strength, the resulting thickness will be approximately 5 mm. The PVC tubes are then redirected through tubular columns of the canopy structure to reduce the airflow disturbance underneath the canopy as much as possible (Figure 1b).

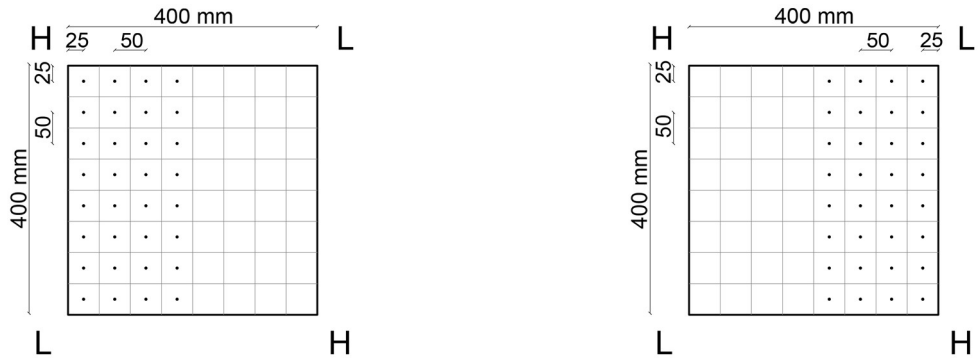

a. Upper face *b. Lower face*

Figure 3: Pressure tap layout of the wind tunnel model.

The layout of the pressure taps is equally spaced over the roof and accounts for the symmetry of the hypar in order to reduce the number of pressure taps (Figure 3). As combining results of different tests is allowed for mean pressures [28], the results of two tests with 180° rotation are combined according to this symmetry to fully cover the pressure distribution over the roof. The pressure taps of the slightly curved hypar were placed at the left half of the model for the upper face and at the right half for the lower face and therefore two 180° rotated tests are needed to obtain net Cp-valus. For the highly curved hypar the pressure taps are located at the left half of the model for both upper and lower face and thus net Cp-values can be obtained with one single test, and two 180° rotated tests are needed to fully cover the roof. In the case that instantaneous values are needed, and pressures should hence be recorded in one single test, it is self-evident to increase the number of taps. Nonetheless, a consideration has to be made between the required number of taps and the thickness of the roof. Mark that significantly increasing the number of taps will give a problem in placing all PVC tubes next to each other, and therefore cause the thickness of the canopy to increase 2 mm for an additional layer of PVC tubes.

2.2. Fabrication process

First the authors tried to 3D-print part of a thin duo-pitched roof with internal airtight channels (Figure 4) from an stl-file containing the virtual model of the roof structure including the internal channels (Figure 4a). The model was printed with a Dimension 1200es 3D printer, with a printable area of 254 mm x 254 mm x 305 mm and a layer thickness of 0,1778mm (Figure 4b). This 3D-printer uses a soluble support material, what allows dissolving the support material by submerging the printed model in a temperature and agitation-controlled water-based solution of the SCA1200 support removal system. However, the internal air channels of 1 mm in diameter tend to be uncontrollable and clog up.

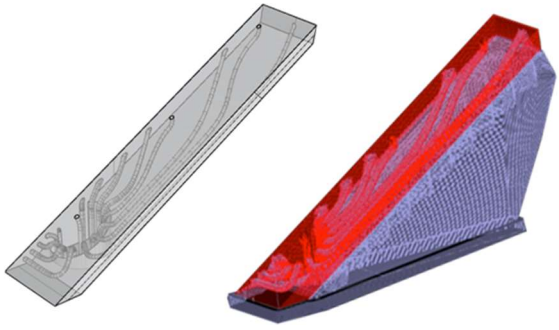

a. Virtual model *b. Layer model 3D-printer*

Figure 4: 3D-printed test piece part of duo-pitch roof.

Nonetheless, 3D-printing is often used to print the envelope of complex wind tunnel models. The printed model should then be further equipped with pressure taps by craftsman. For closed building envelopes, the airtight passageways that connect the pressure taps to the pressure transducers can be easily placed afterwards, but it is not feasible at the moment to implement these airtight passageways inside thin shelled models that are 3D printed. The only option to implement these tubes inside 3D-printed thin shell models is to print the upper and lower face separately, then manually place the airtight passageways and seal the upper and lower face of the canopy together as done in [37] to create 1/1 replicas of roofing tiles. De facto, these printed models will have a substantial thickness for the rigidity under wind loading, while providing the required internal space to place the taps and airtight passageways inside the hollow shell. This is a fairly complex approach and even small leakages can influence the results.

As a solution, the double curved thin shell models are made out of Vubonite [38], a glass-fibre reinforced inorganic phosphate cement, in a CNC-milled mould. This production process allows the fabrication of double curved thin shell models with a large freedom of curved shapes, while preserving sufficient rigidity and resistance to the wind loads during wind tunnel testing.

2.2.1. Mould for roof structure

At first the model of the roof (Figure 5a) and the mould (Figure 5b) have been virtually modelled in Rhinoceros and Inventor. The low corners of the roof are elevated 115 mm and the high points 165 mm. The mould is formed from two parts, a top and a bottom part, fitting perfectly together. Limitations in the machining equipment led to the use of two layers for each part because the total height exceeded the allowed workspace. Consequently, both parts are assembled from two layers of 49 mm thick that are milled from a 50 mm tick high density PUR foam plate. The first mm was milled away to have both parts perfectly matching. After the milling process (Figure 5d) the layers are aligned and glued manually one on top of the other. The two mould parts are sand down and polished by hand to remove some small flaws of the milling process and to achieve a satisfactory smoothness after which the moulds are lacquered.

The milling process is simulated and the G-codes are written in Deskproto (Figure 5c). Here, the different milling operations and their corresponding tools, paths, diameters, feed and plunging rates are defined. In the absence of an automatic tool changer the entire milling process is done with the same 8mm flat tip milling head, because

manually changing the cutting tool would require reprogramming the null point of the work piece resulting inevitably in deviations and mismatches. The milling process for each mould layer is composed of four milling operations. First a roughing operation that takes away large parts of material in a short amount of time (layer height of 5 mm, toolpath overlap of 33% and skin of 2mm), followed by a first finishing operation (toolpath overlap of 33% and skin of 0,5mm), a second finishing operation (toolpath overlap of 66%) to create a smooth surface and finally, a contouring operation to cut the mould layers loose. Mark that the milling process could proceed more efficient with a three- or five-axis CNC-milling machine with an automatic tool changer. This would allow to mill the upper and lower parts of the mould from one piece, with ameliorated refinements. However, at all times a proper balance should be considered between milling time and finishing details.

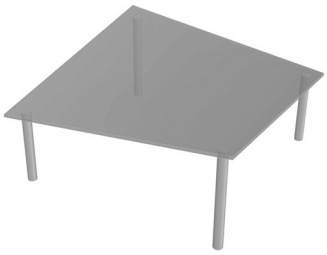

a. Virtual model of the canopy structure.

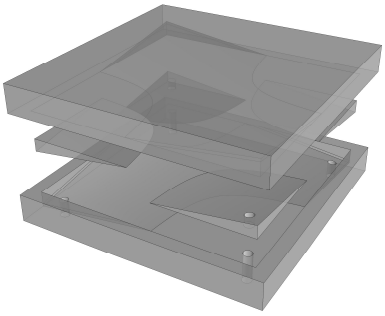

b. Virtual layered mould.

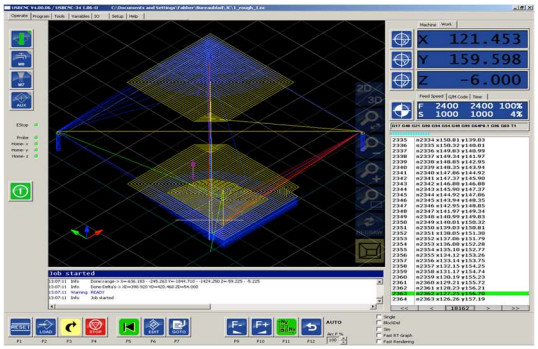

c. Milling operations for the Gantry CNC mill.

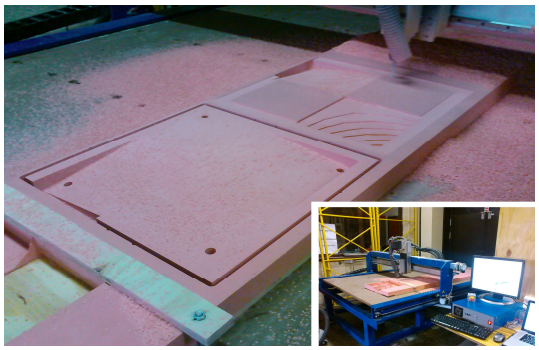

d. Milling process using a Gantry CNC mill.

Figure 5: Fabrication process of mould for the double curved thin shell roof structure using a Gantry CNC mill.

2.2.2. Roof structure

32 Channels of 2mm in diameter are drilled in the upper face of the mould and 30 in the lower face of the mould to fix the PVC tubes at the location of the pressure tap during the pouring and curing process. The channels are drilled perpendicular to the surface to ensure correct measurement of the wind pressure (Figure 6a).

Both parts of the mould are greased with beeswax to make sure that the model releases from the mould after drying. Thereafter, a glass-fibre gauze with randomly oriented glass-fibres (30 gr/m^2) is placed for a smooth surface finishing, followed by a glass-fibre mat (300 gr/m^2) to ensure the stiffness and strength of the model, both impregnated with the inorganic phosphate cement matrix (Figure 6b). The PVC tubes are put through the provided holes in the upper and lower face of the mould to fix the measuring points during the pouring process. Then they are redirected through the columns in a sequence that avoids them folding tight or getting clenched when closing the mould (Figure 6c).

The mould is filled with inorganic phosphate cement matrix while vibrating on a Syntron Magnetic Vibrator V50 D1 at 50 HZ on vibration amplitude level 4 to remove air bubbles from the model and to improve the pouring process (Figure 6d). After pouring the model is vibrated for 10 more minutes at the same settings to ensure nearly all air to be removed from the matrix. The model is dried for one night at ambient temperature after which it is post-cured for six to twelve hours in an oven at 50 °C. After the post-curing process, the model is released from its mould and the protruding tubes are cut off on the level of the corresponding roof faces, the roof edges are rounded, surfaces are polished and small flaws are manually concealed.

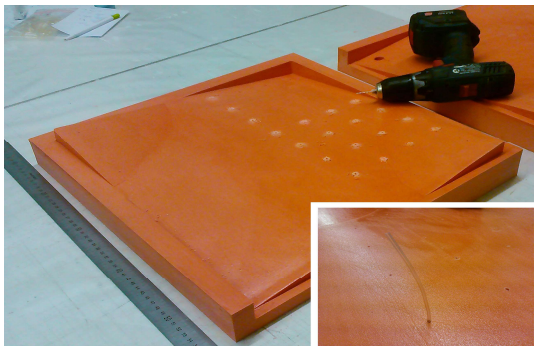

a. Drilling of the holes for the airtight PVC tubes.

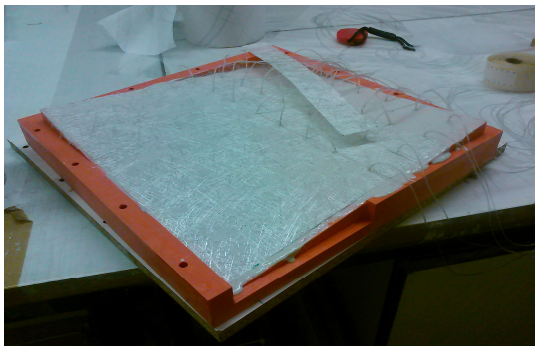

b. Placing the glass-fibre gauze (30 gr/m^2) and mat (300 gr/m^2).

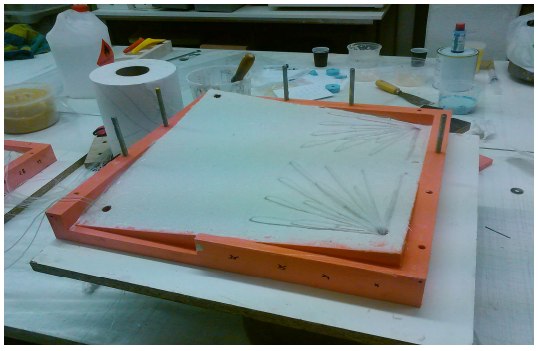

c. Redirecting the PVC airtubes through the columns.

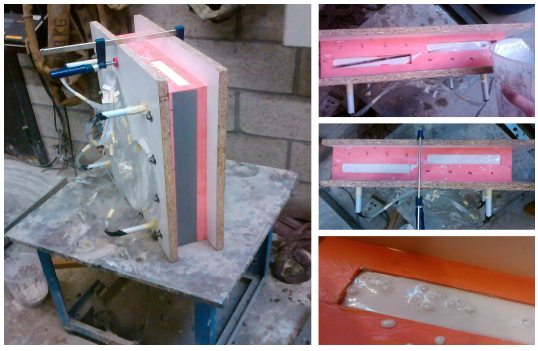

d. Pouring up the mould while vibrating.

Figure 6: Fabrication process of the double curved thin shell roof structure.

2.2.3. Base structure

The wooden base has a void providing sufficient space to connect the redirected tubes to a pressure scanner that will be mounted under the wind tunnel. The void is created by gluing four mitred slats of 18 mm thick on a square plate of 500 x 500 x 5 mm that has been laser cut. This base plate has four circular holes at 75 mm offset from the edges, wherein the tubular columns supporting each corner of the hypar will be clamped (Figure 7).

The wooden base can be secured in the wind tunnel by screws and angle profiles to fix the model in place and transfer the applied wind forces. Furthermore, for each model removable wall elements are laser cut and secured onto the wooden base by angle profiles and screws, allowing them to be added and removed depending on the situation that has to be investigated.

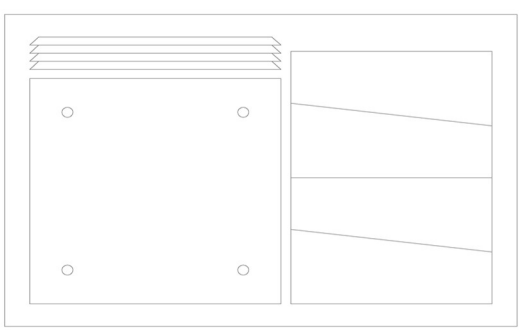

a. CAD®-drawing of base and wall elements

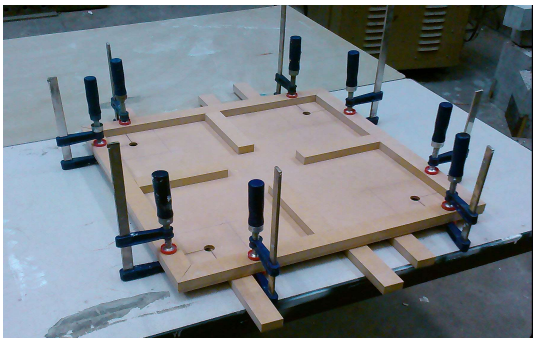

b. Assembly wooden base

Figure 7: Fabrication process of the base structure

2.2.4. Assembly

The double curved thin shell model is mounted on the four PVC tubular columns connecting the inorganic phosphate cement roof and the wooden base (Figure 8). The columns are placed at an offset of 25 mm from each roof edge. The hollow columns have two functions: they transmit the wind loads that act on the roof faces to the base plate and redirect the PVC tubes that are implemented in the roof to the void space that is provided in the base. All elements are glued to ensure stability and adequate load transmission under dynamic wind loading. The PVC columns are clamped into the provided holes in the base structure to ensure resistance against uplift. The wooden base can be secured in the bottom plate of the wind tunnel by screws and angle profiles to fix the model in place and dissipate the applied wind forces.

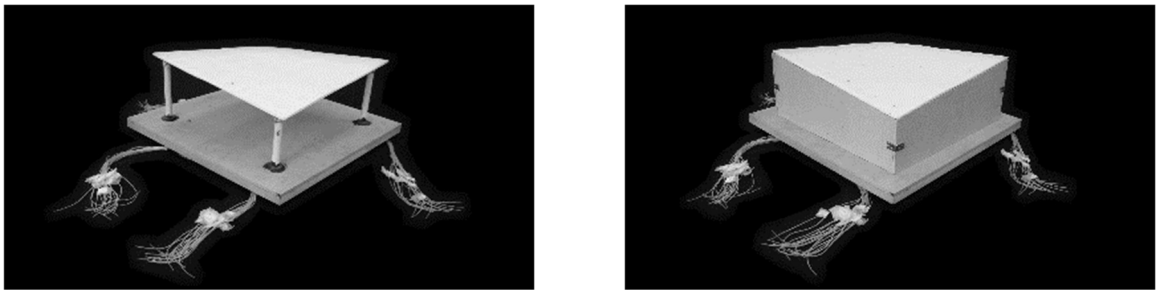

a. Hypar canopy configuration *b. Hypar building roof configuration*

Figure 8: Wind tunnel model of the double curved thin shell hypar canopy and roof.

3. Wind tunnel testing

The wind tunnel tests are performed in an industrial open-circuit wind tunnel at the department of Applied Mechanics at the Vrije Universiteit Brussel. The wind tunnel has a test section of 12 m long, 2 m wide and 1 m high. The models are ground-mounted and subject to the natural boundary layer of the wind tunnel. The test conditions are listed in Table 1.

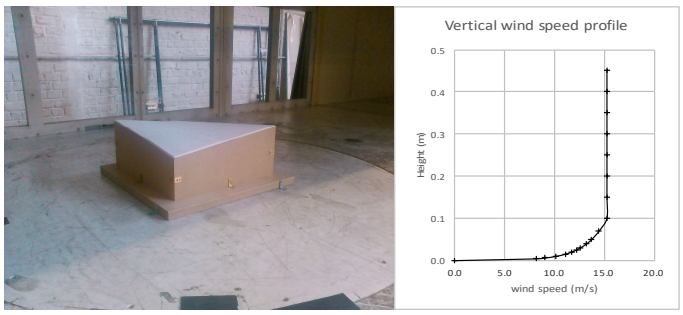

Model	Floor mounted
Maximal tunnel blockage	3,75%
Wind direction	0° - 360°, steps of 15°
Flow type	Intrinsic boundary layer of wind tunnel
Wind velocity	15 m/s
Atmospheric pressure	100146,3 ± 5,66 Pa
Relative humidity	63 ± 0,1%
Temperature	21,9 ± 0,04 ℃
Air density	1,18992 kg/m^3
Number of samples	500
Sampling frequency	10 Hz
Sampling length	50 s

Table 1: Wind tunnel testing conditions.

Pressure measurements are recorded by a computer controlled Scanivalve, type ZOC33/64 Px 10" H_2O at a sampling frequency of 10 Hz and for a sampling length of 50 s. This electronic valveless pressure-scanning module has one reference pressure channel and 64 measuring channels, with an accuracy of 0,15% on 2490,82Pa over its full range. The wind tunnel experiments are performed at a reference wind speed of 5, 10 and 15 m/s and for 360° orientations with increments of 15°. Each experiment is repeated at least 3 times to show consistency in the recorded results, and to exclude potential anomalies. The recorded pressures are made dimensionless and used to create pressure coefficient distribution charts by considering the geometry and the pressure tap layout of the wind tunnel model:

$$C_p = \frac{P - P_0}{\frac{1}{2} * \rho * V^2} \quad (1)$$

where C_p is the pressure coefficient, P the pressure at the measuring tap, P_0 the reference pressure, ρ the air density and V the reference velocity.

3.1. Flat roof

To validate the accuracy of the thin shell wind tunnel models, a flat roof model is made according to the same methodology and tested in the wind tunnel (Figure 9). The results from these wind tunnel experiments are used to validate the experiments and to create a reference-testing field for tests on the hypar model. A flat roof is chosen because it is well studied in literature, while for the hypar experimental wind tunnel results are barely available, and experimental real scale results do not exist.

a. Flat roof canopy configuration. *b. Flat building roof configuration.*

Figure 9: Wind tunnel model of the thin shell flat canopy and roof.

The pattern of the Cp-distribution over the flat roof (Figure 10a) corresponds to the simplified Cp-distributions that are presented by the Eurocode for flat roofs [4]. Largest suction values are found at the upwind edges, with slightly larger values near the upwind corners. Then suction reduces gradually towards the downwind zones. Furthermore, largest peak values are recorded at the upwind edges (in Figure 10a represented by the standard deviation on the Cp-values), what corresponds to the larger difference between peak and average values presented by the Eurocode at these zones. For the flat roof, the experimental results of the Cp-distributions are compared to those presented in [39]. In [39] a flour-mounted cube is tested in both a statistically uniform flow and a boundary layer with a height of ten times the height of the cube, using an open-circuit wind tunnel. Comparison is made to the results under boundary layer flow in [39], there the height of the intrinsic boundary layer of the wind tunnel in our experiment cannot be neglected. In this study, mean pressure measurements

were made over a 20 cm cube, using a multibank inclined manometer, but the pressure tap distribution is not mentioned. The recorded mean Cp-values in a wind tunnel experiment are presented in a graph along the symmetry line of the floor mounted cube with its edge perpendicular to the angle of attack of the boundary layer flow. One can see that the Cp- values along the symmetry of the flat roof correspond to those of the floor mounted cube (Figure 10b). Largest suction values are in both cases present at the upwind edges with Cp- values around -1,0. Thereafter suction reduces towards the downwind zones with values close to -0,1 in [39] and -0,2 in our case.

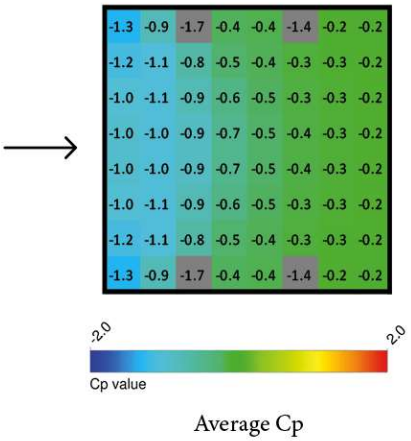

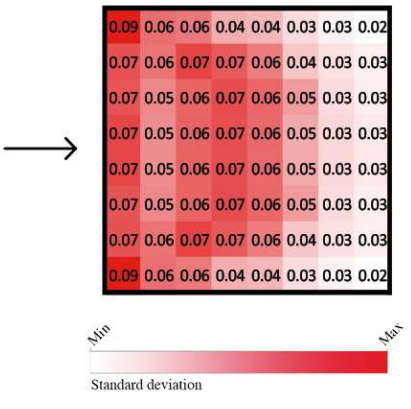

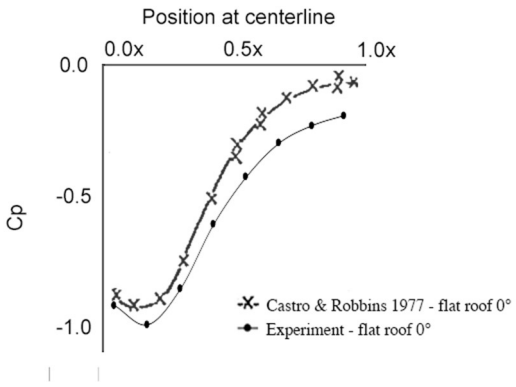

a. Mean Cp,e-distribution and standard deviation over the flat roof.

b. Comparison of the mean Cp,e-values over the flat roof at the centerline along the flow.

Figure 10: Cp,e-distributions over the flat roof.

The conformity between the experimentally obtained Cp-distributions for the flat roof and the floor mounted cube demonstrates the usefulness of the fabricated wind tunnel models and the wind tunnel testing set-up. The general Cp-distributions correspond well. The individual Cp-values differ for approximately 0.2, but rather similar variations are established by several independent studies for the Silsoe cube as stated in [40]-[42]. These deviations could be attributed to the difference in height to span ratio of the roof and the flow field between our case and the floor mounted cube, and furthermore some differences and anomalies in the models (amount and location of pressure taps, detailing of edges, roughness of the surface and imperfections) and the testing conditions (slightly off axis orientations, local turbulences and experimental flaws).

3.2. Flat canopy

For the canopy, the mean Cp-distributions and standard deviations are shown over the upper face and lower face of the canopy (Figure 11 and Figure 12). The results are compared to the mean Cp-distributions presented in [40] for a floor mounted flat canopy. According to the authors' knowledge, no Cp-distributions over both faces of flat canopies with square ground plans are available in literature. Therefore, the Cp-distributions over the upper and lower face of the flat canopy are compared to the mean Cp distributions presented in [43] over a canopy with a rectangular ground plan with a large width. In [43] a 1/40 scale model of a rectangular flat canopy of 12 m by 6 m and a height of 3 m was tested in a boundary layer flow that corresponds to a terrain type II, using a closed-circuit wind tunnel. The model had 63 taps over each face of the roof, with a denser distribution close to the short edges. The geometrical patterns in mean Cp-distribution show some differences for both the upper and lower face of the canopy. For the upper face (Figure 11), the general trend in the Cp-distribution is rather similar, with largest suction at the leading edge, decreasing suction values towards the leeward zone and a little increase in suction near the downwind edge. The larger suction values in [43] (Figure 11b), could be attributed to the different height to span ratio and the different flow field. Next to this, the difference in width between both cases indicates a significant width effect to take place at the edges parallel to the flow. In (Figure 11b) significant circular zones of nearly zero suction are visible near the downwind side of the parallel edges, which are not present our case with a square ground plan.

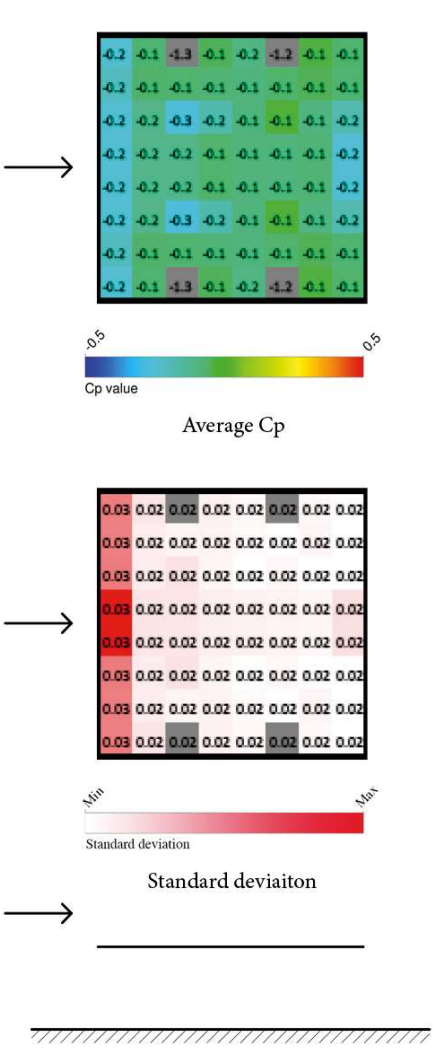

a. Mean Cp-distribution and standard deviation over the upper face of flat canop.

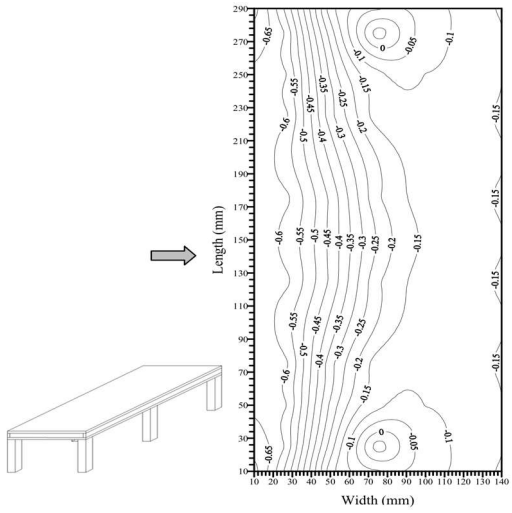

b. Mean Cp-distribution over the upper face of the flat canopy in [43].

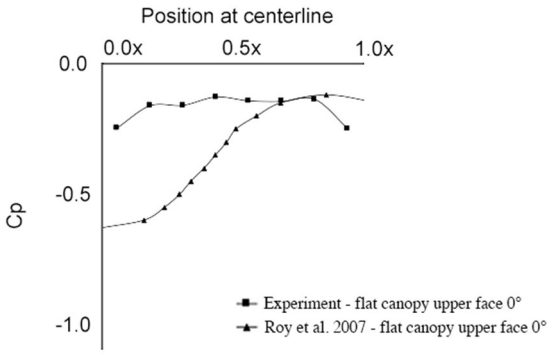

c. Comparison of the mean Cp-values over the upper face of the canopy at the centerline along the flow.

Figure 11: Cp-distributions over the upper face of the flat canopy.

For the lower face (Figure 12), the influence of the building height is more important and affect the flow pattern under the canopy and therefor the pressure distribution over the lower face of the canopy. Although, for both faces of the canopy significant lower suction values are recorded at the leading edge and over the upwind zones of the canopy. This can be seen as a direct result of the lower thickness of the inorganic phosphate cement roof model of only 5 mm at a scale of 1/25, what is only a fourth of the 20 mm thickness of the model assembled from perplex sheets at a scale of 1/40 in [43]. On a real scale this difference corresponds to an almost 6,5x smaller thickness of the roof. Nonetheless, a part of this difference, could be attributed to the different height to span ratio and the different flow field. Furthermore, a similar width effect as found for the upper face is visible near the edges parallel to the flow at the lower face of the wide canopy (Figure 12b).

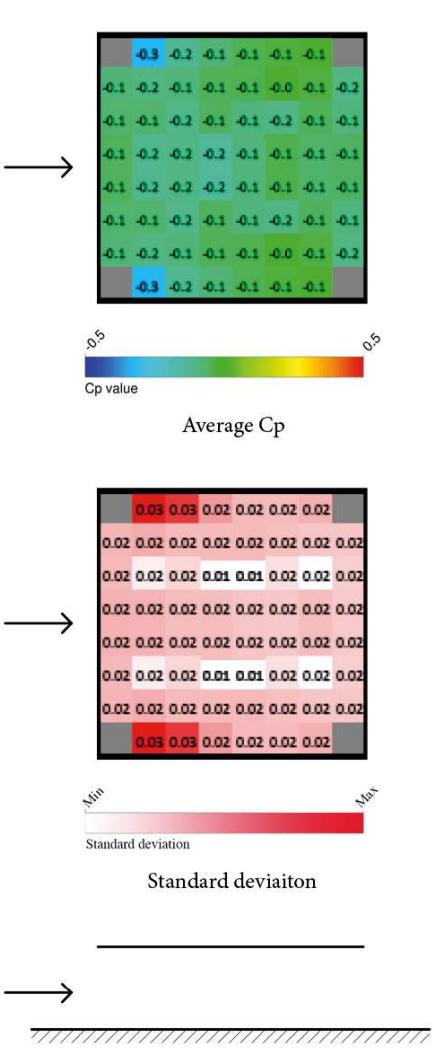

a. Mean Cp-distribution and standard deviation over the lower face of the flat canopy.

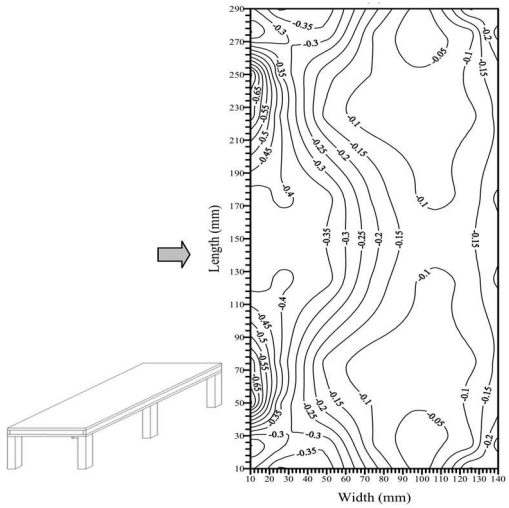

b. Mean Cp-distribution over the lower face of the flat canopy in [43].

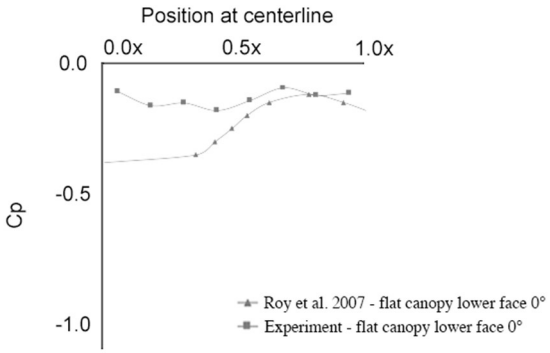

c. Comparison of the mean Cp-values over the lower face of the canopy at the centerline along the flow.

Figure 12: Cp-distributions over the lower face of the flat canopy.

Figure 13 illustrates the evolution of the Cp-distribution along the symmetry line over the upper face of the flat roof and the canopy of our experiments, the flat canopy in [43] and a thin flat plate in [44]. From this figure can be seen that: the smaller the area of the upwind faces or thickness of the upwind edges perpendicular to the flow, the lower the amount of blocked air that has to be redirected over and under the roof, and thus the smaller the separation at the upwind edges. For the roof, most of the blocked air flow at the upwind walls is forced over the building, what results in very high suction values at the upwind edges of the roof. For the canopy in [43] the amount of blocked air is a lot smaller than for the roof and is redirected over and under the canopy, resulting in

lower suction values compared to the roof. For the thin shell wind tunnel models, even less air flow is blocked and redirected over and under the canopy, resulting in even smaller suction values.

Suction values decrease even closer to 0 for very thin plates [44], with almost constant suction values over both faces of the canopy. This can be explained based on the thin airfoil theory [45] and aerodynamic studies of airfoils and flat plates [44][46]. The total lift of a flat plate and symmetrical airfoils with zero degrees inclination to the flow equals 0, due to identical Cp-distributions over both faces of the flat plate or the symmetrical airfoil. The computational study in [44] was performed using RANS simulations. The results show very low mean Cp-values close to 0, over both faces of a flat plate with a thickness to chord length ratio of 2% and an angle of attack of 0°, with locally slightly larger suction values near the upwind edge. The Cp-values are very close to the local mean Cp-values over both faces of the canopy in our study that has a thickness to chord length ratio of 1.25%. Furthermore, [44] also shows lower Cp-values for the flat plate compared to the NACA 0012 airfoil, what can be attributed to less redirection of the flow. This has also been shown in the NACA technical report 824 [46], where the influence of the thickness of symmetrical NACA airfoils is investigated. In general, the larger the airfoil thickness, the larger the perturbation of the free flow and thus the redistribution of the flow, what results in larger total drag and larger local Cp-values over the upper and lower face of the airfoils. Therefore, these thin shell wind tunnel models allow to yield more realistic wind pressures and Cp-values over very thin canopy structures due to their very low thickness compared to the currently used wind tunnel models for canopy structures.

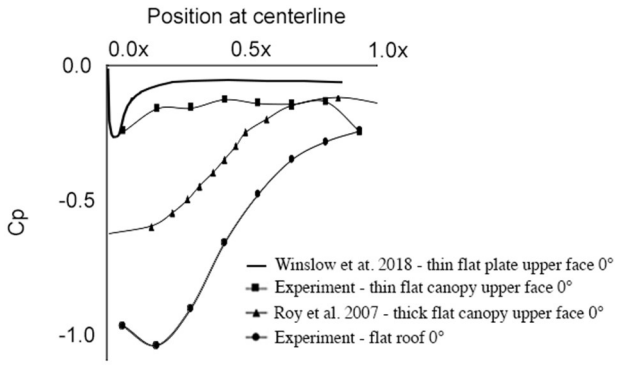

Figure 13: The Comparison of the mean Cp-values over the flat roof, the upper face of the flat canopy, the flat canopy in [43] and the thin plate in [44] at the centreline along the flow illustrates the influence of the roof/canopy thickness on the Cp-values.

3.3. Hypar roof

In Figure 14, the mean Cp-distributions and standard deviation are shown for the slightly curved hypar roof with the high corner under attack (Figure 14a) and compared to the results presented in [12] for hypar roofs with circular ground plan (Figure 14b).

In [12], mean and peak Cp-distributions are shown for hypar roofs with arched edges and square, rectangular and circular ground, each for two surface curvatures and two roof heights. The circular plans are considered for comparison, because the geometry of these models fits aerodynamically best to our case when the high apex is under attack (Figure 14b). The models with circular ground plan have 109 pressure taps on the roof, arranged in 16 polar arrays, with higher density at the roof edge and along the two main curves of the hypar. The experiments have been made in a boundary layer wind tunnel with an atmospheric boundary layer of terrain type III. Model p.11 fits geometrically best with our case. The models have almost the same roof height, with slightly lower curvature of the hypar roof between its high corners. The mean aerodynamics show rather similar evolution along the centerline (Figure 14c), with largest suction values near the upwind high apex, then a reduction of the suction values over the central zone and again a slight increase at the downwind high apex. However, due to the different topology of the hypar with high and low corners, larger suction values are found near the upwind high corner and this suction spreads further along the roof edges and drops quickly along the centerline, which has also been indicated for the floor mounted cube. Furthermore, it can be seen that the standard deviation is larger at the locations of largest suction values. This indicates that peak values are more important at these upwind locations, what is also noticed in [12], and has been validated by peak factor analysis in [9].

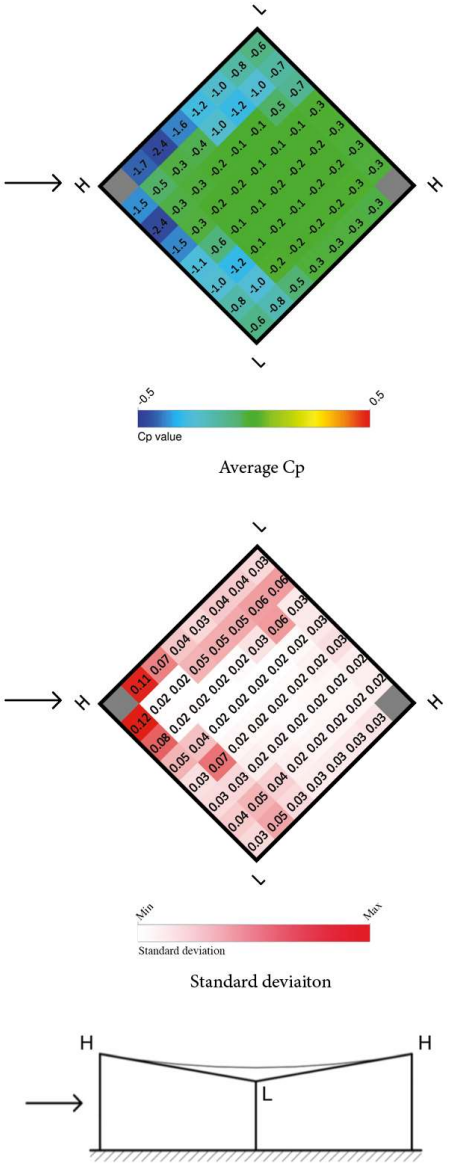

a. Mean Cp,e-distribution and standard deviation over the slightly curved hypar roof.

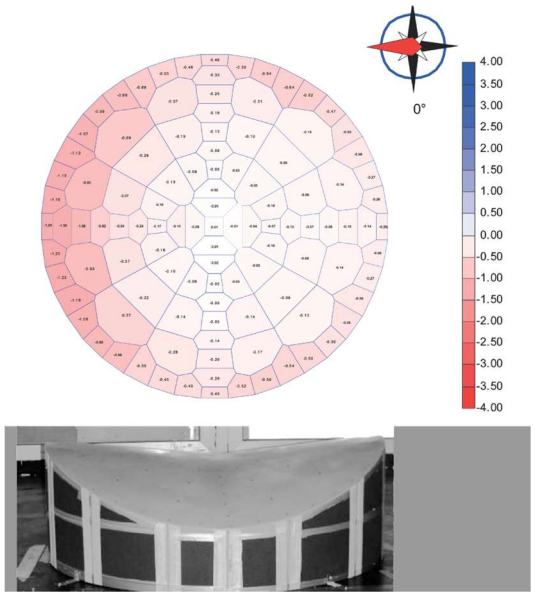

b. Mean Cp,e-distribution over the hypar roof in [12].

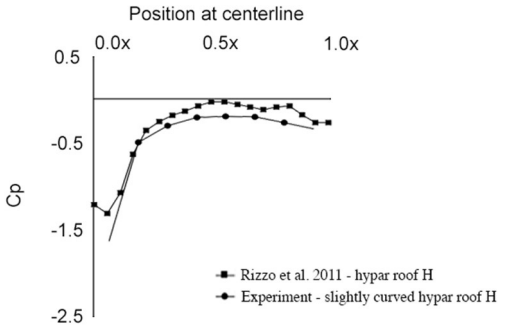

c. Comparison of the mean Cp,e-values at the centreline of the slightly curved hypar roof along the flow.

Figure 14: Mean Cp,e distributions over the slightly curved hypar roof.

Figure 15, presents the mean Cp-distribution for the highly curved hypar roof with its high corner under attack (Figure 15a) and compares the results to the mean Cp-distribution in [8] for a similar hypar roof (Figure 15b).

In [8] Cp-distributions are presented over the hypar roof of an exhibition hall, with its low corners almost at ground level and with inclined walls (Figure 15b). The scale model of the exhibition hall with an hypar roof with a large curvature has been tested in the constant flow field of an open WT. The roof was equipped with 117 pressure taps, from which only 20 could be connected at the same time, and were read out manually one by one from a water pressure meter. The patterns in the pressure distribution over the highly curved hypar roof (Figure

15a) correspond rather well to those presented in [8], although Cp-values differ due the different height of the roof. In both studies, largest suction values and largest standard deviations are recorded at the upwind high corner and edges. Larger values are recorded due to the higher position of the roof compared to [8], which causes a larger perturbation of the free flow. Just behind the prevailing suction values at the upwind corner a significant decrease in suction is observed. Then suction-values reduce further towards the central zones of the roof, and positive pressure values develop due to the higher curvature. Finally, suction slightly increases again towards the downwind corner and similar suction values are reported at the downwind corner for both studies.

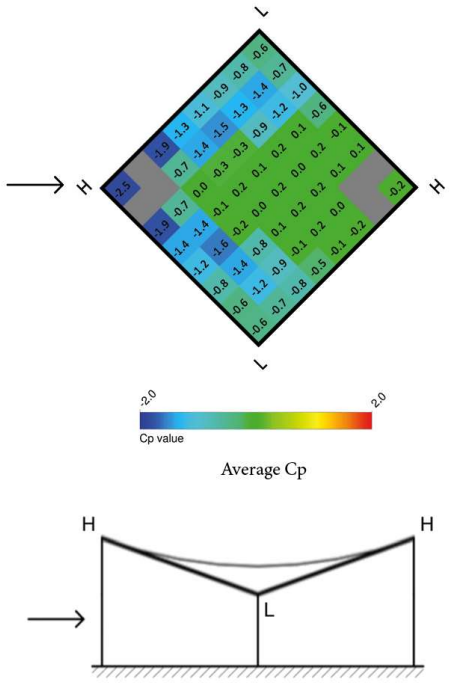

a. Mean Cp,e-distribution over the highly curved hypar roof.

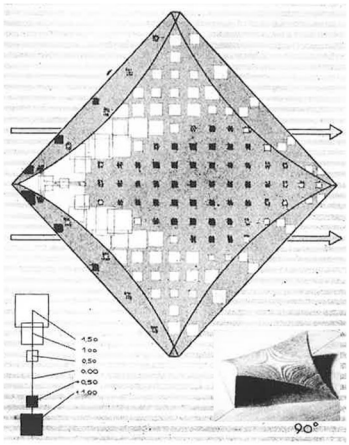

b. Mean Cp,e-distribution over the hypar roof in [8].

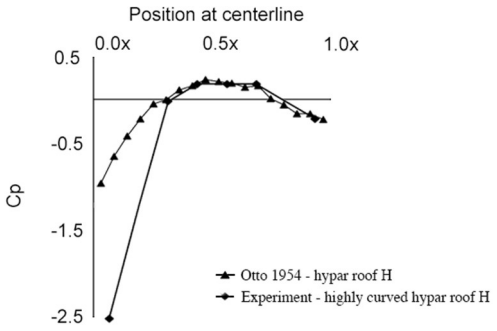

c. Comparison of the mean Cp,e-values at the centreline of the highly curved hypar roof along the flow.

Figure 15: Mean Cp,e distributions over the highly curved hypar roof.

3.4. Hypar canopy

The mean Cp-distributions over the upper and lower face of the hypar canopy are shown in Figure 16 for the slightly curved hypar and in Figure 17 for the highly curved hypar. For the upper face of the slightly curved hypar canopy (Figure 16a), largest suction is found close to the upwind corner, then suction reduces close to zero and

even small positive pressure develops at the central zones of the roof and suction slightly increases again near the downwind high corner. For the lower face (Figure 16b) the opposite behavior takes place. Suction increases over the central areas of the lower face and slightly reduces near the downwind corner. This can be explained by the Venturi effect under the hypar canopy, i.e. as the canopy and the base act as funnel/neck causing an increase of the flow velocity and a drop in ambient air pressure.

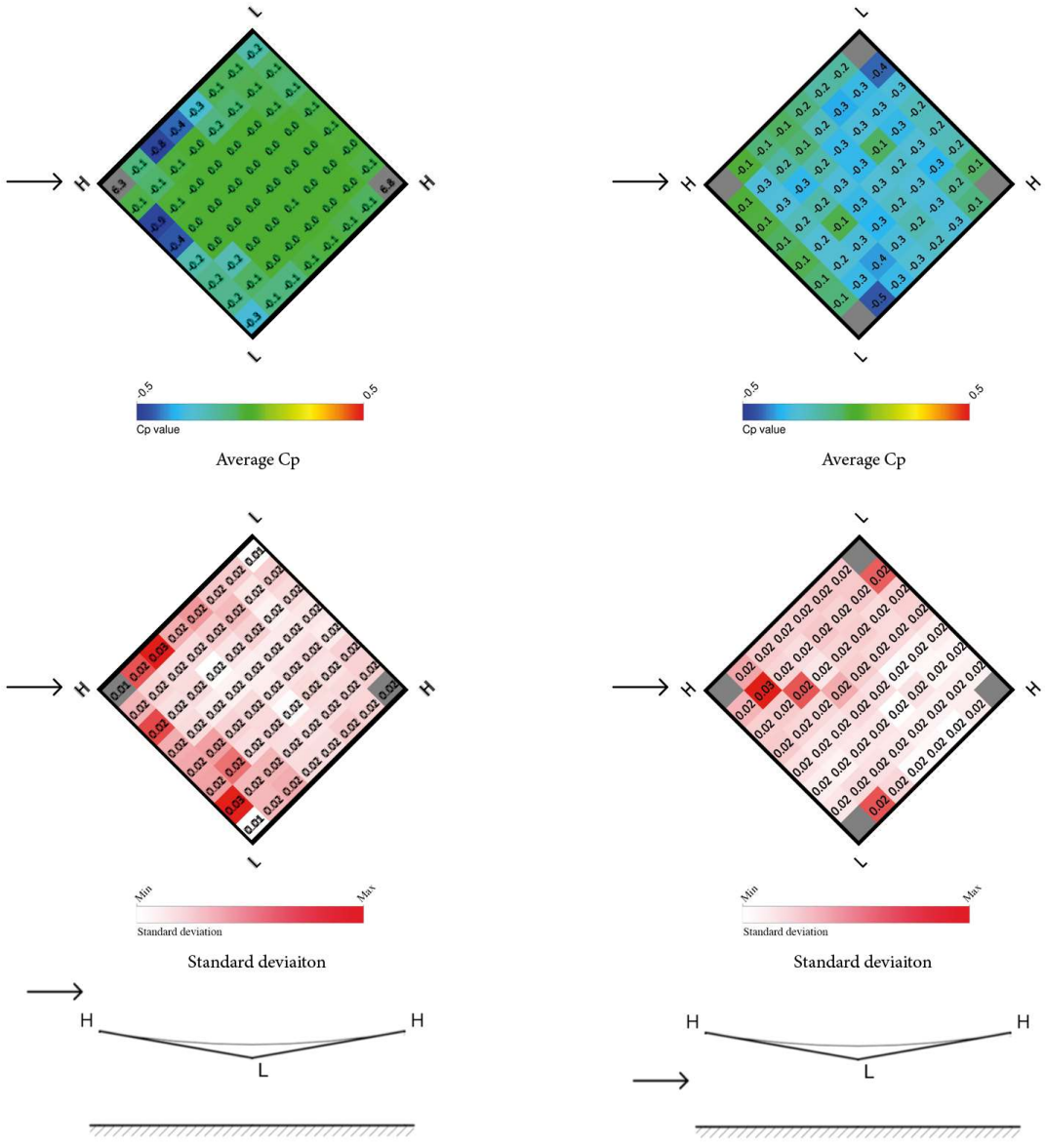

a. Upper face of the slightly curved hypar canopy.

b. Lower face of the slightly curved hypar canopy.

Figure 16: Mean Cp-distributions and standard deviations over the upper and lower face of the slightly curved hypar canopy.

For the highly curved hypar canopy (Figure 17), similar results are found, but Cp-values become more expressive due to the higher curvature of the hypar. Positive pressure develops over the central areas of the upper face (Figure 17a) of the highly curved canopy and suction values are larger over the lower face (Figure 17b) compared to the slightly curved hypar canopy.

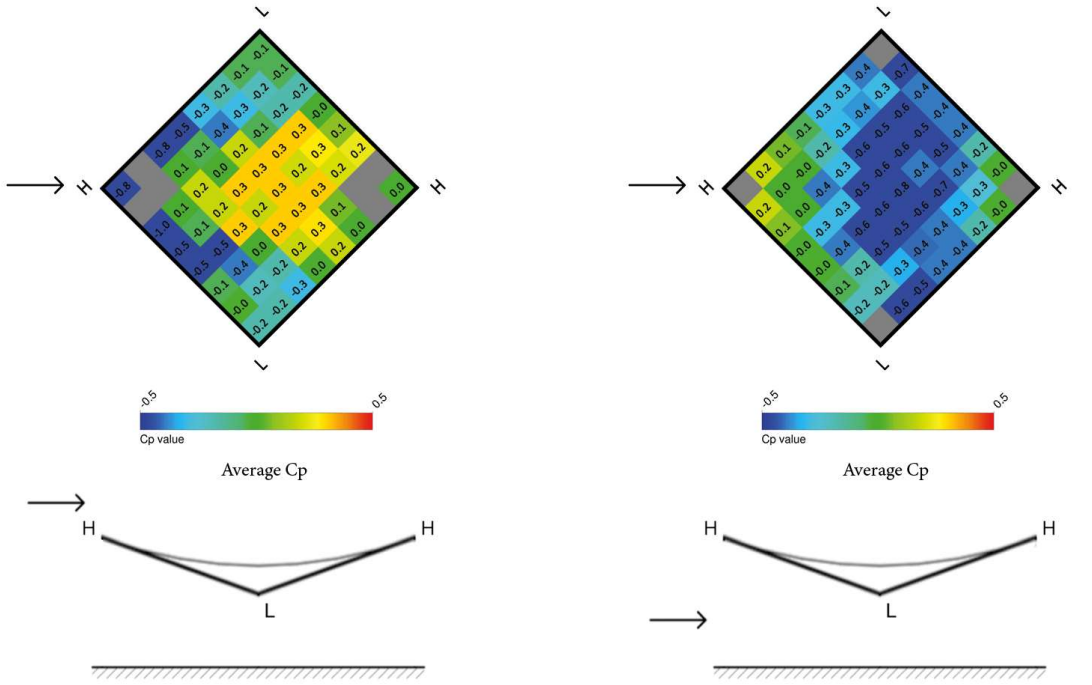

a. Upper face of the highly curved hypar canopy. *b. Lower face of the highly curved hypar canopy.*

Figure 17: Mean Cp-distributions over the upper and lower face of the highly curved hypar canopy.

Figure 18 illustrates the evolution of the Cp-distribution along the symmetry line over the upper face of the hypar roof and the hypar canopies of our experiments. From this figure can be easily seen that the suction values over the upper face of the slightly curved hypar canopy are lower compared to the slightly curved hypar roof (Figure 18a), what has also been noticed for the flat canopy compared to the flat roof. For the highly curved hypar the pressure values are larger for the canopy compared to the roof (Figure 18b). In general suction-values are smaller and pressure values are larger for the canopy, due to the smaller perturbation of the flow, while largest suction zones remain at the same position as found for the roof configuration.

a. Slightly curved hypar roof and canopy

b. Highly curved hypar roof and canopy

Figure 18: The comparison of the mean Cp-values over the hypar roof and canopy at the centreline along the flow illustrates the influence of the roof/canopy thickness on the Cp-values.

4. Conclusion

The presented fabrication methodology for scaled wind tunnel models of glass fibre composite is convenient and accurate for double curved thin shell wind tunnel models that allow simultaneous pressure measurements over both faces of a thin canopy. The methodology can be easily adopted for various organically shaped membrane or shell structures and allows implementing different materials as long as the structure provides sufficient resistance to wind loads during wind tunnel testing. Canopy structures with a thickness of only 5mm are made, what is 4 times smaller compared to conventional canopy wind tunnel models with a thickness of approximately 20 mm. This small thickness will become particularly important for aerodynamic wind tunnel studies of the built environment that are typically performed at a scale of 1/500 or smaller. The reduced thickness causes a smaller perturbation of the air flow and results in more realistic values close to the upwind edges, which has been validated by comparison to literature. The obtained Cp-distributions for the flat roof are consistent literature and fall within the variation of independent studies for the Silsoe cube [39]-[42]. The results for the flat canopy show more relevant Cp-values for very thin canopies, and relate to the numerical results obtained for a thin plate, with lower suction values at the upwind zones. The lower suction values are a direct result of the smaller surface area of the upwind edge, that causes less redistribution of the flow over and under the canopy and therefore aerodynamics thin plates. The Cp-distributions over the slightly curved and the highly curved hypar roof show good correlation to the few available studies in literature, considering the different curvature and ground plans of the hypar roofs studied in literature. The Cp-distributions show that the pressure distribution becomes more

expressive with increasing curvature. With the high corner under attack, the slightly curved hypar roof is fully loaded by suction, while for the highly curved hypar larger suction values are recorded at the upwind high corner and pressure develops at the central zones of the roof. Finally, first results are shown for the slightly curved and the highly curved hypar canopy with their high corner under attack. The Cp-distributions over both canopies show similar behaviour as over the roof configurations. Largest suction zones remain at the same position, but in general suction-values are smaller and pressure values are larger for the canopy due to the smaller perturbation of the free flow. The presented study proves the usefulness of the fabricated wind tunnel models and the presented prototyping methodology can therefore facilitate experimental wind load analysis on very thin often organically shaped canopy structures.

Acknowledgements

This research is conducted under PhD-fellowship of the Research Foundation Flanders (FWO-Vlaanderen).

Furthermore, the authors would like to thank the COST Association for facilitating a European framework through meetings of Working Group 5 – From material to structure and limit states: codes and standardisation – of the COST Action TU1303 Novel Structural Skins.

Bibliography

[1] Gorlin, W. B., 2009. Wind Loads for Temporary Structures: Making the Case for Industrywide Standards. Journal of Architectural Engineering 15 (2), 35–36.

[2] Forster, B., Mollaert, M. (eds), 2004. European Design Guide for Tensile Surface Structures. TensiNet, Brussels.

[3] ASCE (American Society of Civil Engineers), 2013. ASCE/SEI 7-05: Wind Loads - Minimum Design Loads for Buildings and Other Structures.

[4] CEN (European Committee for Standardizations), 2005. EN 1991-1-4:2005. Eurocode 1: Actions on structures - Part 1-4: General actions - Wind actions.

[5] Stathopoulos T., Baniotopoulos C.C. (eds), Wind Effects on Buildings and Design of Wind-Sensitive Structures. CISM International Centre for Mechanical Sciences 493. Springer, Vienna.

[6] Nagai, Y., et al., 2012. Wind Response of Horn-Shaped Membrane Roof and Proposal of Gust Factor for Membrane Structures. Journal of the International Association for Shell and Spatial Structures 53 (3), 169-176.

[7] Hincz, K., Gamboa-Maruffo, M., 2016. Deformed Shape Wind Analysis of Tensile Membrane Structures. Journal of Structural Engineering 142 (3).

[8] Otto, F., 1954. Das hängende Dach. Ph.D. Thesis, Technische Universität Berlin, Berlin.

[9] Rizzo, F., Barbato M., Sepe, V., 2018. Peak factor statistics of wind effects for hyperbolic paraboloid roofs. Engineering Structures 173, 313-330.

[10] Rizzo, F., Ricciardelli, F., 2017. Design pressure coefficients for circular and elliptical plan structures with hyperbolic paraboloid roof. Engineering Structures 139, 153-169.

[11] Rizzo, F., Sepe, V., 2015. Static loads to simulate dynamic effects of wind on hyperbolic paraboloid roofs with square plan. Journal of Wind Engineering and Industrial Aerodynamics 137, 46-57.

[12] Rizzo, F., et al., 2011. Wind action evaluation on tension roofs of hyperbolic paraboloid shape. Engineering structures 33, 445–461.

[13] Sun, X., et al., 2008. Wind Tunnel Tests on the Aeroelastic Behaviors on Pretensioned Saddle-Shaped Suspended Roofs. Presented at: The 6th International Colloquium on Bluff Body Aerodynamics and Applications.

[14] Takeda, F., Yoshino, T., Uematsu, Y., 2014. Design Wind Force Coefficients for Hyperbolic Paraboloid Free Roofs. Journal of Physical Science and Application 4 (1), 1–19.

[15] Xuanyi, Z., et al., 2013. Research on wind-induced responses of a large-scale membrane structure. Earthquake Engineering and Engineering Vibration 12 (2), 297-305.

[17] Irwin H., Wardlaw, L., 1979. A Wind Tunnel Investigation of a Retractable Fabric Roof for the Montreal Olympic Stadium. In: Proceedings of 5th International Conference on Wind Engineering, 925–938.

[17] Cook, M. J., 1981. Wind Tunnel Tests for Large Surface Stresses Structure in Kuweit. Buro Happold Engineers Ltd.

[18] Balz, M., Fildhuth, T., 2004. Wind Loading on Stadia Roof Structures. Schlaich Bergermann and Partners. In: Mollaert, M., et al., (eds), Proceedings of the TensiNet Symposium 2003: Designing Tensile Architecture, 140-149.

[19] El-ashkar, I., Novak, M., 1983. Wind Tunnel Studies of Cable Roofs. Journal of Wind Engineering and Industrial Aerodynamics 13 (1-3), 407–419.

[20] Luo, J., Han, D., 2009. 3D wind-induced response analysis of a cable-membrane structure. Journal of Zhejiang University 10 (3), 337–344.

[21] Mall, F., 2014. Ermittlung von Windlasten auf Bauwerke mit Hilfe von CFD-Berechnungen. Master Thesis, Hochschule für Technik, Wirtschaft und Gestaltung Konstanz, Radolfzell.

[22] Michalski, A., 2009. Simulation leichter Flächentragwerke in einer numerisch generierten atmosphärischen Grenzschicht. Ph.D. Thesis, Technischen Universität München, Munchen.

[23] Wüchner, R., Kupzok, A., Bletzinger, K.-U., 2006. Simulation of fluid-structure -interaction with free form membrane structures using an implicit coupling scheme with adaptive under relaxation. Presented at: The European Conference on Computational Fluid Dynamics.

[24] Kupzok, A., 2009. Modeling the Interaction of Wind and Membrane Structures by Numerical Simulation. Ph.D. Thesis, Technischen Universität München, Munchen.

[25] Michalski, A., et al., 2011. Validation of the computational fluid-structure interaction simulation at real-scale tests of a flexible 29 m umbrella in natural wind flow. Journal of Wind Engineering and Industrial Aerodynamics 99, 400-413.

[26] Rank, E., et al., 2005. Wind loads on lightweight structures: Numerical simulation and wind tunnel tests. GAMM-Mitteilungen 28 (1), 73-89.

[27] Xuanyi, Z., et al., 2013. Research on wind-induced responses of a largescale membrane structure. Earthquake Engineering and Engineering Vibration 12 (2), 297–305.

[28] Isyumov, N., 1999. Wind Tunnel Studies of Buildings and Structures. ASCE.

[29] Alan G. Davenport Wind Engineering Group, 2007. Wind Tunnel Testing: A General Outline. University of Western Ontario, London.

[30] CUR (Civieltechnisch Centrum Uitvoering Research en Regelgeving), 2005. CUR aanbeveling 103: Windtunnelonderzoek voor de bepaling van ontwerpbeslissingen op (hoge) gebouwen en onderdelen ervan.

[31] Barlow, J.B., Rae, W.H., Pope, A., 1999. Low-Speed Wind Tunnel Testing. 3rd edition, John Wiley & Sons.

[32] Adelnia, R., Aghanajafi S., Daneshmand S., 2006. Evaluation of Surface Finish Effect on Aerodynamic Coefficients of Wind Tunnel Testing Models. In: Proceedings of the 4th WSEAS International Conference on Fluid Mechanics and Aerodynamics.

[33] Artzi, D., Kroll, E., 2011. Lessons from Wind Tunnel Models made by Rapid Prototyping. Rapid Prototyping Journal 17 (5).

[34] Daneshmand, S., Adelnia, R., AghanajafiI, S., 2006. Comparison between FDM Model and Steel Model as Wind Tunnel Testing Models. In: Proceedings of the 6th WSEAS International Conference on Robotics, Control and Manufacturing Technology, 36-41.

[35] Daneshmand, S., Adelnia, R., AghanajafiI, S., 2006. Evaluating Aerodynamic Characteristics of Wind-Tunnel Models Produced by Selective Laser Sintering Method. In: Proceedings of the 4th WSEAS International Conference on Fluid Mechanics and Aerodynamics, 12-17.

[36] Hildebrand, R., et al., 2003. Development of a low cost, rapid prototype, lambda wing- body, wind-tunnel model. Presented at: The 21st Applied Aerodynamics Conference.

[37] Smith, D. J., Masters, F. J., Chowdhury, A. G., 2016. Investigating a wind tunnel method for determining wind-induced loads on roofing tiles. Journal of Wind Engineering and Industrial Aerodynamics 155, 47-59.

[38] Symbion nv, http://www.vubonite.com, Retrieved May 17, 2018.

[39] Castro, I. P., Robins, A. G., 1977. The flow around surface mounted cube in uniform and turbulent streams. Journal of Fluid Mechanics 79, 307-335.

[40] Richards, P. J. , Hoxey, R. P., Short, L. J., 2001. Wind pressures on a 6 m cube. Journal of Wind Engineering and Industrial Aerodynamics 89 (14-15), 1553-1564.

[41] Franke, J., 2007. Introduction to the Prediction of Wind Loads on Buildings by Computational Wind Engineering (CWE). In: Stathopoulos, T., Baniotopoulos, C. C. (eds.). Wind Effects on Buildings and Design of Wind-Sensitive Structures. Springer, Vienna, 67-103.

[42] Abohela, I., Hamza, N., Dudek, S., 2012. Validating CFD Simulation Results: Wind flow around a surface mounted cube in a turbulent channel flow. Presented at: The 28th Conference Opportunities, Limits & Needs Towards an environmentally responsible architecture.

[43] Roy, A. K., Ahuja, A. K., Gupta, V. K., 2007. Wind pressure distribution on flat canopy roof. Presented at: Recent advances in civil engineering.

[44] Winslow, J., et al., 2018. Basic Understanding of Airfoil Characteristics at Low Reynolds Numbers (10^4–10^5). Journal of Aircraft 55 (3), 1050-1061.

[45] Anderson, J. D. Jr., 2010. Chapter 4: Incompressible Flow over Airfoils, Section 4.7 Classical Thin Airfoil Theory: The Symmetric Airfoil. In: Anderson J.D. Jr. (ed), Fundamentals in Aerodynamics, fifth edition, McGraw-Hill Education, 338-347.

[46] Abbott, I. H., Von Doenhoff, A. E., Stivers, L. Jr. 1945. NACA Technical Report 824. National Advisory Committee for Aeronautics Langley Aeronautical Lab, Langley Field.